

LARGE-SCALE MODES IN A ROTATING
ATMOSPHERE WITH RADIATIVE-CONVECTIVE
INSTABILITY AND WISHE

ZELJKA FUCHS AND DAVID J. RAYMOND

April 28, 2005

Physics Department and Geophysical Research Center, New Mexico Institute of Mining
and Technology, Socorro, New Mexico

email: tzeljka@nmt.edu

Abstract

A highly simplified parameterization of diabatic processes is applied to linearized equations on an equatorial beta plane. The diabatic processes include moist convection, cloud-radiation interactions (CRI), and wind-induced surface heat exchange (WISHE). The precipitation rate is assumed to increase linearly as the vertically averaged saturation deficit decreases.

The modeled modes are Matsuno's normal modes, i. e., Kelvin waves, mixed Rossby-gravity waves, Rossby waves, and inertio-gravity waves, and an additional mode which we call a slow moisture mode. All of the Matsuno modes are damped and remain stable even when CRI and WISHE are turned on. Their phase speeds don't vary much from Matsuno's adiabatic values except for very long wavelength Kelvin and Rossby modes, for which the phase speeds are reduced compared to the adiabatic values. The slow moisture modes are stationary and unstable under CRI, while WISHE causes them to propagate. Under CRI and WISHE together the slow moisture modes are unstable and eastward propagating for long wavelengths and slowly moving relative to the mean flow for short wavelengths. The dispersion relations of the slow moisture modes are one of nearly constant or decreasing frequency with increasing wavenumber. The most important model parameter is the tropospheric moisture relaxation time scale, chosen to be one day.

The model failed to explain the observed phase speeds of convectively coupled Matsuno modes. We suggest, following Mapes (2000), that other dynamics, more realistic than the one including only the first baroclinic mode, may be responsible for these modes.

1. Introduction

Large-scale disturbances such as equatorially trapped waves couple with convection in a way that we still don't understand. As this coupling plays a large role in synoptic variability in the tropics, it is essential to understand the basic mechanism for it. Since the earliest satellite observations of cloudiness (Chang 1970), it is known that there are westward propagating synoptic scale disturbances in the ITCZ (intertropical convergence zone) over the tropical oceans. Just before the first satellite observations, the basic theory for equatorially trapped waves expressed in terms of the shallow water approximation was developed by Matsuno (1966). The wave modes identified by Matsuno are Kelvin waves, mixed Rossby-gravity waves, Rossby waves and inertio-gravity waves.

There have been many recent observational studies of convectively coupled waves. The most recent and complete are those by Straub and Kiladis (2002), Wheeler et al. (2000), and Wheeler and Kiladis (1999). Much of the variance in space and time of deep tropical cloudiness observed from satellites is explained very well by the adiabatic shallow water theory in which convection is accounted for by reducing the effective static stability of the fundamental baroclinic mode. However the greatest variability observed in the tropics is due to the Madden-Julian oscillation (MJO), first discovered by Madden and Julian (1971, 1972, 1994) as a perturbation in surface pressure, cloudiness, precipitation and wind on a time scale of 40-50 days. The MJO is not described by this simple treatment of convection nor will our model shine more light into its basic physical mechanism.

Emanuel (1987) suggested that deep convection in the tropics exists in statistical equilibrium with large scale disturbances, as opposed to the then widely accepted theory that convection is driven by the selective release of CAPE (convective available potential energy). This approach implies that there are additional processes which are responsible for coupling of the deep convection and the large scale disturbances. Emanuel (1987) and Neelin et al. (1987) suggested that the mechanism called WISHE (wind induced

surface heat exchange) is responsible for a variety of the wave instabilities in the tropics. Neelin and Yu (1994) developed an analytical model for the convectively coupled tropical modes following the idea of WISHE using the Betts-Miller moist convective adjustment parameterization with an adjustment time of 2 hours. They found two main classes of modes, the first of which decay so rapidly that the dynamical processes have no time to adjust and the second which have the time scale set by the large-scale dynamics. The former are of no physical interest while the latter include an eastward propagating mode that becomes unstable under the influence of WISHE.

Raymond (2001) developed a numerical model where cloud-radiation interactions (CRI) are the primary mechanism for producing the large-scale disturbances. Over uniform SST the instabilities occur only when CRI is turned on. When there is an equatorial SST maximum the resulting disturbances look like the observed MJO. Together with CRI, the key condition for the existence of the modeled MJO-like modes is a lag of several days between heavy precipitation and the onset of enhanced surface fluxes. The reason for the lag is that it takes time to humidify the troposphere via surface fluxes, and therefore to increase the precipitation rate.

Fuchs and Raymond (2002) developed a simple model in order to understand better the results of Raymond (2001). The basic idea was to create a model which incorporates sensitivity of convection to moisture, CRI, and WISHE. Surface sensible heat fluxes are ignored as they are small over the tropical oceans. For the sake of simplicity the model was posed in a nonrotating atmosphere.

The CRI enters into the model via tropospheric moisture: more moisture implies more clouds, which then leads to more suppression of upward radiation and enhancement of the upward motion. WISHE comes in as a propagation mechanism in the presence of mean easterly flow. However, the sensitivity of convection to moisture is, in our opinion, a little bit trickier. Observational studies (Raymond and Wilkening 1985; DeMott and

Rutledge 1998) and numerical models (Tompkins and Craig, 1998; Raymond and Zeng, 2004) suggest that the precipitation produced by convection is a strong function of the relative humidity, where heavier precipitation occurs with higher humidity. In that sense Raymond (2000b) suggested a very simple relationship between humidity and precipitation over the warm tropical oceans. Fuchs and Raymond (2002) used that hypothesis and parametrized precipitation rate as a function inversely proportional to the vertically averaged saturation deficit. Even though the CAPE dependence is included in the precipitation parameterization, in that increased CAPE results in increased precipitation, the modeled results remained qualitatively the same with or without CAPE sensitivity. The model assumes a vertical structure consisting of only the first baroclinic mode. The model also assumes a rigid lid at the tropopause.

The modeled modes include damped, eastward and westward-propagating gravity waves and an unstable mode. The unstable mode is stationary when CRI is turned on and eastward-propagating in the presence of a mean easterly flow with both WISHE and CRI. However when CRI and WISHE are turned off the mode is stationary and damped. For realistic wavelengths it is damped at the same rate as the stationary moisture mode of Sobel et al. (2001) who analyzed shallow water equations under the assumption of a weak temperature gradient with an imposed diabatic heating. In their linearized moist model the convective heating is controlled by the horizontal moisture advection. Surface fluxes and radiative heating are ignored. In the nonrotating case they derive a stationary moist mode. Sobel and Bretherton (2003) examined the interactions of large-scale waves with deep convection in the idealized nonrotating mesoscale simulations with fixed radiative cooling and imposed heating. Their model produced convectively coupled gravity waves and a stationary wave with a strong signal in moisture field in the presence of a mean easterly flow of -5 m/s. The stationary wave resembles to great extent the stationary moisture mode of Sobel et al. and the stationary mode of Fuchs and Raymond in the case

when CRI and WISHE are turned off.

The gravity waves in Fuchs and Raymond (2002), although damped, did not slow down for realistic wavelengths. This is in disagreement with Neelin and Yu (1994), as their gravity modes slow down in a response to reduced static stability due to parameterization of deep convection. As the model (Fuchs and Raymond) was done in nonrotating atmosphere, the results are not comparable to the observational results of Wheeler and Kiladis (1999). The purpose of this paper is to expand the model to the equatorial beta plane. Our goal is to model the convectively coupled Matsuno modes as observed by Straub and Kiladis (2002), Wheeler et al. (2000), and Wheeler and Kiladis (1999) as well as to see what happens to the slow moisture mode in a model that brings us closer to the realistic world.

Section 2 describes the model and its assumptions. Section 3 presents the results, while the discussion of the results and the conclusions are given in section 4.

2. Model

The model presented in this article is an extension to an equatorial beta plane of the Fuchs and Raymond (2002) model. We explore the sensitivity of convection to moisture, CRI, and WISHE for the first baroclinic vertical mode. The Boussinesq approximation is used with a rigid lid at the tropopause. The governing equations are linearized about a state of rest.

2.1. Thermodynamic assumptions

The thermodynamics of the model, i.e. moist convection, CRI and WISHE come into the governing equations as the source terms of the buoyancy, s_B , moisture, s_Q , and equivalent potential temperature, s_E .

In our model that includes only the first baroclinic mode where the assumed vertical

structure of the source terms is: $(s_B, s_Q, s_E) = (s_b, s_q, s_e) \sin(mz)$. The parameter $m = \pi/h$ is a vertical wavenumber and h is the depth of the troposphere. This assumption is weak as in reality there are moisture perturbations at the surface, however, it is necessary for the simplicity of the model. Vertically integrated source terms of our model are then:

$$s_b \propto \int_0^h s_B dz = P - R \quad (1)$$

$$s_q \propto \int_0^h s_Q dz = E - P \quad (2)$$

$$s_e \propto \int_0^h s_E dz = E - R \quad (3)$$

where P , E and R are scaled perturbations in the precipitation rate, the surface evaporation rate, and the vertically integrated radiative cooling rate.

The source term for equivalent potential temperature s_e depends on the perturbations in surface evaporation rate minus vertically integrated radiative cooling rate. The mixing ratio source term s_q depends on perturbations in surface evaporation rate minus the precipitation rate. Buoyancy source term $s_b = s_e - s_q$ then depends on perturbations in precipitation rate minus the vertically integrated radiative cooling rate.

The precipitation rate is assumed to increase linearly as the vertically averaged saturation deficit decreases or as the vertically averaged mixing ratio increases. The relaxation rate of the moisture profile toward equilibrium is α . In addition Fuchs and Raymond (2002) assumed that increased CAPE results in increased precipitation with a relaxation rate μ . Although the model represented in this article in its calculation toward the dispersion relation includes the CAPE effect, the results are given only for the $\mu = 0$ case as there is no qualitative change in the results for nonzero μ .

The radiative cooling rate is assumed to decrease linearly as the mixing ratio increases

as a result of the associated increase in cloudiness. This can best be understood by considering two columns, where one column represents the cloud-free environment and the other is cloudy (Grey, 1973). As the clouds trap the upward radiation, the cloudy region experiences a radiative cooling rate of less than 1 K/day while the clear region has a cooling rate of about 2 K/day. The cloudy region then becomes warmer relative to the clear region which gives rise to positive buoyancy and leads to reinforcing of the preexisting upward motion associated with cloudiness. This mechanism is called cloud-radiation interaction (CRI) and is represented in this model through cloud-radiative parameter, ε .

WISHE comes in through the surface evaporation term that is parameterized using the bulk flux formula for surface evaporation with the assumption of an ambient easterly wind. $\delta = mC\eta\Delta q/2$ is the WISHE parameter used in our model. For more details on parameterization of source terms see Fuchs and Raymond (2002).

The vertical dependence of all the fields as well as the source terms is limited to one vertical mode: $(w, b, q) \propto \sin(mz)$, $(u, v, p) \propto \cos(mz)$ where again $m = \pi/h$ is a vertical wavenumber, and h is the depth of the troposphere. For consequences of considering only the first baroclinic vertical mode see discussion and conclusions.

Finally the thermodynamic equations of the model are as follows:

$$\frac{\partial b}{\partial t} + \Gamma_B w = \alpha(1 + \varepsilon)q - \mu b \quad (4)$$

$$\frac{\partial q}{\partial t} + \Gamma_Q w = u\delta - \alpha q + \mu b \quad (5)$$

$$\frac{\partial e}{\partial t} + \Gamma_E w = u\delta + \alpha\varepsilon q \quad (6)$$

where $e = g\frac{\theta_e}{\theta_0}$ is the scaled equivalent potential temperature, $b = g\frac{\theta}{\theta_0}$ is the buoyancy and $q = \frac{gLr}{C_p\theta_0}$ is the scaled mixing ratio. Note that $e = b + q$. θ_e is the perturbation from

a reference profile of equivalent potential temperature θ_{e0} , θ is the perturbation from a reference profile of potential temperature θ_0 , r is the mixing ratio perturbation from a reference profile r_0 , L is the latent heat release of evaporation and C_p is the specific heat of air at constant temperature. Furthermore dry static stability and moist static stability are related through $\Gamma_E = \Gamma_B + \Gamma_Q$. Γ_B is the square of Brunt-Vaisala frequency, $\Gamma_B = \frac{g}{\theta_0} \frac{d\theta_0}{dz}$, $\Gamma_Q = \frac{gL}{C_p \theta_0} \frac{dr_0}{dz}$, and moist static stability $\Gamma_E = \frac{g}{\theta_0} \frac{d\theta_{e0}}{dz}$ is assumed to have a typical value of $\Gamma_E = 0.1\Gamma_B$ (Emanuel et al. 1994). For numerical values of parameters used in the model see Table 1.

Assuming that $e = b + q$, we get the relationship between the source terms $s_e = s_b + s_q$. One of the equations (4) - (6) is therefore redundant.

2.2. Nondimensionalized linearized governing equations

We have nondimensionalized in a different way than Matsuno (1966) in order to maintain consistency with Fuchs and Raymond (2002). Matsuno scaled time and length using $[T] = (1/c\beta)^{1/2}$, $[L] = (c/\beta)^{1/2}$ where $c = \frac{\Gamma_B^{1/2}}{m}$ is the speed of free Kelvin wave and $\beta = \frac{f}{y}$ is the so-called Rossby parameter, taken as constant. However the key parameter in our treatment of convection and precipitation is the moisture relaxation time $\alpha^{-1} \sim 1$ d. Following Fuchs and Raymond (2002), we use α^{-1} as the time scale in the nondimensionalization. For details on nondimensionalization see Table 2.

The components of the nondimensionalized momentum equations are:

$$\frac{\partial u}{\partial t} - \beta y v + \frac{\partial p}{\partial x} = 0 \quad (7)$$

$$\frac{\partial v}{\partial t} + \beta y u + \frac{\partial p}{\partial y} = 0 \quad (8)$$

The nondimensionalized hydrostatic and continuity equations are:

$$\frac{\partial p}{\partial z} = b \quad (9)$$

$$\frac{\partial u}{\partial x} + \frac{\partial v}{\partial y} + \frac{\partial w}{\partial z} = 0 \quad (10)$$

The nondimensionalized buoyancy, moisture, and equivalent potential temperature equations are:

$$\frac{\partial b}{\partial t} + w = (1 + \varepsilon)q - (\sigma - 1)b \quad (11)$$

$$\frac{\partial q}{\partial t} + \frac{\Gamma - 1}{1 + \varepsilon}w = \frac{\Lambda}{1 + \varepsilon}u - q + (\sigma - 1)b \quad (12)$$

$$\frac{\partial e}{\partial t} + \frac{\Gamma + \varepsilon}{1 + \varepsilon}w = \frac{\Lambda}{1 + \varepsilon}u + \varepsilon q \quad (13)$$

- $\sigma = (\alpha + \mu)/\alpha$ is a dimensionless parameter that includes moisture and buoyancy relaxation rates. We give the results with $\mu = 0$ or $\sigma = 1$ which implies that precipitation rate doesn't depend on CAPE.
- $\Gamma = (\Gamma_E + \varepsilon\Gamma_Q)/\Gamma_B$ is a dimensionless static stability that includes the cloud-radiation interactions and the latent heat release. We include the effects of radiation by setting $\varepsilon = 0.2$, see Fuchs and Raymond (2002). The dimensionless static stability is then $\Gamma = -0.1$. The radiative-convective instability exists in our model as long as $\Gamma \leq 0$, $\varepsilon \geq 0.11$.
- $\Lambda = \delta(1 + \epsilon)/\alpha\Gamma_B^{1/2}$, is a dimensionless parameter that includes the effects of wind-induced variations in surface heat fluxes, calculated to be $\Lambda = -0.4$, see Fuchs and

Raymond (2002). As $\varepsilon = 0.2$, a simple dimensional analysis shows that CRI doesn't play an important role in this parameter.

2.3. Solution of equations

We assume that all the variables are proportional to $\exp[i(\kappa x - \Omega t)]$ where κ is a dimensionless zonal wavenumber, $\kappa = k\Gamma_B^{1/2}/(\alpha m)$ and $\Omega = \omega/\alpha$ is a dimensionless frequency, k and ω being the dimensional versions.

The equations (7) - (12) represent a closed system of equations with six unknowns: nondimensionalized perturbations of horizontal and vertical wind components u ; v ; and w ; the nondimensionalized kinematic pressure perturbation p ; b ; and q . We take the equivalent potential temperature equation to be redundant and omit it.

Substituting the assumed x and t dependence and simplifying we get a differential equation of second order for v :

$$\frac{\partial^2 v}{\partial y^2} + ay \frac{\partial v}{\partial y} + (b + dy^2)v = 0 \quad (14)$$

where

$$a = \frac{\beta \Lambda i}{\Omega (\Gamma - i\Omega)} \quad (15)$$

$$b = \frac{\beta \Lambda i}{\Omega (\Gamma - i\Omega)} - \frac{\beta \kappa}{\Omega} - \kappa^2 - \frac{i\Omega^3 - i\Lambda \kappa - \sigma \Omega^2 + i\varepsilon \Omega (\sigma - 1)}{\Gamma - i\Omega} \quad (16)$$

$$d = \frac{\beta^2 [i\Omega^2 - \sigma \Omega + i\varepsilon (\sigma - 1)]}{\Omega (\Gamma - i\Omega)} \quad (17)$$

In obtaining (14) we had to divide by the quantity A :

$$A = (\Gamma - i\Omega)\kappa^2 - i\Lambda\kappa + i\Omega^3 - \sigma\Omega^2 + i\varepsilon\Omega(\sigma - 1), \quad (18)$$

so we have the auxiliary condition $A \neq 0$.

The solution to (14) is:

$$v(y) = C e^{-\left(\frac{a}{4} \pm \frac{1}{4}(a^2 - 4d)^{1/2}\right)y^2} H_n(y) \quad (19)$$

where $H_n(y)$ is the Hermite polynomial of the n th order. Since we are considering the wave motions near the equator, the boundary conditions are:

$$v \rightarrow 0, \text{ when } y \rightarrow \pm\infty \quad (20)$$

The equation (14) with the boundary conditions (20) poses an eigenvalue problem. The boundary conditions are satisfied only when the constant $\pm(2b - a)/(a^2 - 4d)^{1/2}$ is equal to an odd integer:

$$\pm \frac{2b - a}{(a^2 - 4d)^{1/2}} = 2n + 1 \quad (21)$$

where $n = 0, 1, 2, \dots$. For the lowest mode, $n = 0$, we get a dispersion relation:

$$\begin{aligned} \Omega^4 + i\sigma\Omega^3 + [\varepsilon(\sigma - 1) - \kappa^2]\Omega^2 - (\Lambda\kappa + i\Gamma\kappa^2 + \beta\kappa)\Omega - \frac{\beta\Lambda}{2} - i\beta\kappa\Gamma & \pm \\ \beta(\Omega^4 + i\Omega^3(\sigma + \Gamma) + [\varepsilon(\sigma - 1) - \Gamma\sigma]\Omega^2 + i\varepsilon\Gamma(\sigma - 1)\Omega + \frac{\Lambda^2}{4})^{1/2} & = 0 \end{aligned} \quad (22)$$

For simplicity we call the expression under the square-root s :

$$s = \Omega^4 + i\Omega^3(\sigma + \Gamma) + [\varepsilon(\sigma - 1) - \Gamma\sigma]\Omega^2 + i\varepsilon\Gamma(\sigma - 1)\Omega + \frac{\Lambda^2}{4} \quad (23)$$

The sign of $s^{1/2}$ in the dispersion relation (22) is the same as the sign under the

exponential function in the solution for v , equation (19). To obtain the solutions which are equatorially trapped, we require that all the variables decay as we move away from the equator. For v , that condition is satisfied if the real part of the coefficient of y^2 in the exponential function in (19) is negative. That coefficient is:

$$c_f = -\left(\frac{a}{4} \pm \frac{1}{4}(a^2 - 4d)^{1/2}\right) = -\frac{\beta i}{4\Omega(\Gamma - i\Omega)} \left(\Lambda \pm 2s^{1/2}\right) \quad (24)$$

There are eight solutions to the dispersion relation (22) out of which four survive after checking for the right sign of the coefficient c_f . Furthermore two of those four solutions are the solutions to $A = 0$, which is not acceptable. So there are two solutions that exist for the mode $n = 0$ and they correspond to eastward and westward-propagating mixed Rossby-gravity waves.

For $n = 1, 2$ case the situation is much simpler: four modes come out from the dispersion relation which satisfy all the boundary conditions and $A \neq 0$.

2.4. Case with $v = 0$

There is one additional important solution to consider which has $v(x, y) = 0$ everywhere. The equation (14) is therefore inapplicable and this case must be derived directly from the system of equations (7) - (12).

In this case we derive a differential equation of first order for p :

$$\frac{dp}{dy} + \frac{\beta\kappa}{\Omega}yp = 0 \quad (25)$$

with a solution:

$$p(y) = C \exp\left(-\frac{\beta\kappa}{2\Omega}y^2\right) \quad (26)$$

that has to satisfy the same boundary conditions for equatorially trapped waves as in

section 2.3.

The dispersion relation is then:

$$\Omega^3 + i\sigma\Omega^2 - [\kappa^2 - \varepsilon(\sigma - 1)]\Omega - i\kappa^2\left(\Gamma - i\frac{\Lambda}{\kappa}\right) = 0 \quad (27)$$

and the nondimensionalized polarization relations in terms of p are:

$$u = \frac{\kappa}{\Omega}p \quad (28)$$

$$w = -i\frac{\kappa^2}{\Omega}p \quad (29)$$

$$b = -p \quad (30)$$

$$q = \frac{1}{i\Omega - 1} \left(\sigma - 1 + \frac{i\kappa^2(\Gamma - 1) + i\Lambda\kappa}{\Omega(\varepsilon + 1)} \right) p \quad (31)$$

The dispersion relation gives three different modes, stable eastward and westward modes and an unstable eastward mode. When checked for boundary conditions in (26), out of those three modes two survive, both eastward propagating.

3. Results

The dispersion relations for the combined CRI - WISHE case set up by nondimensional parameters: cloud-radiative feedback parameter $\varepsilon = 0.2$, static stability $\Gamma = -0.1$, moisture relaxation $\sigma = 1$, and WISHE parameter $\Lambda = -0.4$; are plotted in Figures 1 - 4. The dimensionless phase speed of the wave modes in plot A is $\Phi = \text{Re}(\Omega/\kappa)$. Plot B shows the dimensionless growth rate.

Figure 1 shows the results of the dispersion relation (27) for case with $v = 0$. The eastward-propagating stable mode is identified as a Kelvin mode. For short wavelengths it has the same phase speed as in Matsuno's case, but slows down for long wavelengths. This mode is damped. The unstable eastward propagating mode is a slow moisture mode.

Figure 2 shows the results of the dispersion relation (22) for $n = 0$ case, nondimensionalized $\beta = 10$, see Table 1. The calculated modes are eastward and westward-propagating mixed Rossby-gravity modes. They are damped. For the westward-propagating mixed Rossby-gravity mode there is a certain value of κ for which the mode characteristics change. For long wavelengths with $\kappa \leq 2.2$, the mode shows characteristics of gravity waves, while for short wavelengths it acts like a Rossby wave.

Figure 3 shows the results of the dispersion relation (22) for $n = 1$ case, $\beta = 10$. There are four modes, eastward and westward-propagating inertio-gravity waves, a Rossby wave and a slow moisture mode. Like the Kelvin mode in Figure 1, the Rossby wave has the same phase speed as Matsuno's in a short wavelength regime, but slows down in the long wavelength regime. The inertio-gravity waves have almost the same phase speed as in the adiabatic case. All modes except the slow moisture mode are stable.

Figure 4 is the same as 3, only for the $n = 2$ case.

The real part of the dimensionless frequency for the slow moisture mode for $v = 0$, $n = 1$, and $n = 2$ is plotted in Figure 5. The mode is highly dispersive.

Figure 6 shows the dimensional dispersion curves for slow moisture modes for $v = 0$, $n = 1$, and $n = 2$ cases for combined CRI-WISHE case. The wavenumber used is the planetary wavenumber $l = k/k_1$, $k_1 = 2\pi/40000 \text{ km}^{-1}$, $l = 1...20$. The physical phase speed of the slow moisture modes is shown in plot A while the imaginary part of the frequency in units of inverse days is shown in plot B. Figure 7 shows the dimensional growth rate of the slow moisture modes for two cases, with WISHE, but without CRI, and with CRI, but without WISHE.

Figures 8 - 10 show the slow moisture mode in the $v = 0$ case for two different relaxation times, the one of one day and the other of two hours. Figure 8 shows the combined CRI - WISHE case, Figure 9 the case where only WISHE is included and Figure 10 the case where CRI is included and WISHE is not.

4. Discussion of results and conclusions

4.1 Discussion

As expected, the slow moisture mode and the Kelvin mode that come out of the $v = 0$ case in a rotating atmosphere correspond to two modes previously found by Fuchs and Raymond (2002) in a nonrotating atmosphere. Rotation allows in addition the generation of the mixed Rossby-gravity waves ($n = 0$ case in Matsuno's notation). For meridional numbers $n = 1$ and $n = 2$ we find inertio-gravity modes, Rossby modes and slow moisture modes. The slow moisture modes for $n = 1, 2$ are stationary and unstable when just cloud-radiation interactions (CRI) are invoked while wind-induced surface heat exchange (WISHE) gives them the propagation mechanism, as in the $v = 0$ case.

Looking in more detail at the slow moisture modes, Figure 6, we see that for long wavelengths, from 15000 to 40000 km, the slow moisture modes propagate eastward with phase speeds from 5 to 18 m/s. For shorter wavelengths the modes significantly slow down and for the wavelengths of 2000 to 4000 km the modes move very slowly relative to the mean flow. The slow moisture modes are unstable under CRI and WISHE effects. When only WISHE is invoked they are unstable only for long wavelengths, while with CRI only the modes show uniform growth rate with the e-folding time of ten days, Figure 7. All of the slow moisture modes are highly dispersive, with the frequency nearly constant or decreasing with increasing wavenumber.

Our modeled Matsuno modes don't differ much from the free Matsuno modes. The

phase speeds of inertio-gravity modes and Rossby modes barely decrease compared to their adiabatic wave speeds; however, they are damped. The Kelvin mode and Rossby mode, also damped, change their phase speeds under the influence of diabatic effects, but given our scaling, only for unrealistically long wavelengths. The Matsuno modes are damped because due to diabatic effects the convection lags the vertical velocity or forcing. A very small lag of convection is enough to shift convective heating to the cold phase of the wave which is then enough to lead to negative correlation of heating and temperature. Negative correlation of heating, represented through our buoyancy source term, and temperature represented by buoyancy leads to decay of the wave. Emanuel et al. (1994) called this mechanism moist convective damping.

4.2. Moisture relaxation time

The most important parameter of our model is the tropospheric moisture relaxation time. It represents time in which a combination of surface fluxes, convergence and precipitation relax the moisture profile to some equilibrium. Based on physical arguments we choose it to be one day; for more details see Fuchs and Raymond (2002). Recently, studies and numerical models confirm that moisture relaxation time is close to that value. Bretherton et al. (2004) analyzed the relationship between water vapor path and surface precipitation rate over the tropical oceans from four years of satellite data. They found that the moisture adjustment time scale in schemes such as Betts-Miller for convective rainfall should be 12 hours for horizontal grid spacings on the order of 300 kilometers. Furthermore Sobel and Bretherton (2003) used their numerical model to estimate the convective moisture time scale under which they model the stationary moisture mode. The estimated value they get for wavelength of 4500 km is 2.5 days. As our model is somewhat similar to that of Neelin and Yu (1994), we were curious to see what happens to our slow moisture modes for different moisture relaxation time scales, as Neelin and Yu used the Betts-Miller

cumulus parameterization assuming an adjustment time of two hours.

We find that our slow moisture modes remain unstable even when we reduce the moisture relaxation time from 1 day to 2 hours. In the case with $v = 0$ (Figure 8), we see that when CRI and WISHE are included, the slow moisture mode propagates with slightly larger dimensional phase speed with the shorter relaxation time, and has larger growth rate. When CRI is turned off and only WISHE is invoked, the slow moisture mode remains unstable and eastward propagating for only large wavelengths: it is unstable up to global wavenumber two for a relaxation time of one day and up to wavenumber six for a two hour relaxation time, Figure (9). On the other hand, when CRI is invoked without WISHE, the mode is stationary and unstable, with larger growth rate for the shorter relaxation time, Figure (10).

In their model Neelin and Yu found a somewhat similar mode to our slow moisture mode. Unlike the Neelin-Yu case, we find, for both relaxation times, slow moisture modes for $n = 1$ and $n = 2$ as well as for the $v = 0$ case. The dispersion relation of Neelin and Yu's modes is different from ours; their unstable mode moves much more rapidly.

4.3 Conclusions

The slow moisture modes come out of our model as the only unstable modes. They are produced by moist processes independent of moisture relaxation time scale over the range of two hours to one day. They are highly dispersive and exist for higher meridional mode numbers as well as for $n = 0$. Cloud-radiation interactions play a key role in destabilizing these modes, with WISHE providing the propagation mechanism as well as additional destabilization.

Aside from the slow moisture modes, our model produced Matsuno's normal modes. The thermodynamic assumptions of the model have little effect on the phase speeds of those modes, but cause them to be damped. Only the Kelvin mode and Rossby

mode change their phase speeds under the influence of diabatic effects, but only for unrealistically long wavelengths. The relaxation time of one day damps these modes significantly less than the relaxation time of two hours.

Why does our model not predict reduced propagation speeds for the Matsuno modes? We can think of nothing really wrong with physical assumptions aside from perhaps the lack of dependence of convection on convective inhibition (CIN). The importance of CIN is discussed by Raymond et al. (2003) based on the study EPIC2001 (Eastern Pacific Investigation of Climate). If there is nothing wrong with thermal assumptions of the model, then there must be something wrong with dynamics, which brings us to the most unrealistic assumption of the model; its vertical structure. The observed convectively coupled Matsuno modes have a “boomerang” thermodynamical structure (Wheeler et al., 2000) which cannot be reproduced by the assumed vertical structure in the present model. Mapes (2000) suggested that the vertical structure of stratiform rain regions should be treated as a separate mode with significantly smaller vertical wavelength than the mode corresponding to the convective rain regions. We have started to work on another model that takes care of the unrealistic dynamics of this model.

Acknowledgments. We thank the anonymous reviewers for their useful comments. This work was supported by National Science Foundation Grant ATM-0352639.

REFERENCES

- Arakawa**, A., and W. H. Schubert, 1974: Interaction of a cumulus cloud ensemble with the large-scale environment. Part I. *J. Atmos. Sci.*, **31**, 674-701.
- Betts**, A. K., 1982: Saturation point analysis of moist convective overturning. *J. Atmos. Sci.*, **39**, 1484-1505.
- Bretherton**, C. S., M. E. Peters, and L. E. Back, 2004: Relationships between water vapor path and precipitation over the tropical oceans. *J. Climate.*, **17**, 1517-1528
- Chang**, C. -P., 1970: Westward propagating cloud patterns in the tropical Pacific as seen from time-composite satellite photographs. *J. Atmos. Sci.*, **27**, 133-138.
- Charney**, J. G., and A. Eliassen, 1964: On the growth of the hurricane depression. *J. Atmos. Sci.*, **21**, 68-75.
- DeMott**, C. A., and S. A. Rutledge, 1998: The vertical structure of TOGA COARE convection. Part II: Modulating influences and implications for diabatic heating. *J. Atmos. Sci.*, **55**, 2748-2762.
- Emanuel K. A.**, 1986: An air-sea interaction theory for tropical cyclones. Part I. *J. Atmos. Sci.*, **43**, 585-604.
- Emanuel K. A.**, 1987: An air-sea interaction model of Intraseasonal Oscillations in the Tropics. *J. Atmos. Sci.*, **44**, 2324-2340.
- Emanuel K. A.**, 1993: The effect of convective response time on WISHE modes. *J. Atmos. Sci.*, **50**, 1763-1775.
- Emanuel K. A.**, J. D. Neelin, and C. S. Bretherton, 1994: On large-scale circulations in convective atmosphere. *Quart. J. Roy. Meteor. Soc.*, **120**, 1111-1143.

- Fuchs, Z.**, and D. J. Raymond, 2002: Large-scale modes of a nonrotating atmosphere with water vapor and cloud-radiation feedbacks. *J. Atmos. Sci.*, **59**, 1669-1679.
- Grabowski, W. W.**, 2003: MJO-like coherent structures: Sensitivity simulations using the cloud-resolving convection parameterization (CRCP). *J. Atmos. Sci.*, **60**, 847-864.
- Grabowski, W. W.**, and M. W. Moncrieff, 2003: Moisture-convection feedback in the Tropics: *submitted to Quart. J. Roy. Meteor. Soc.*
- Grey, W. M.**, 1973: Cumulus convection and larger scale circulations I. Broad-scale and mesoscale considerations. *Mon. Wea. Rev.*, **101**, 839-855.
- Mapes, B. E.**, 2000: Convective inhibition, subgrid-scale triggering energy, and stratiform instability in a toy tropical wave model. *J. Atmos. Sci.*, **57**, 1515-1535.
- Matsuno, T.**, 1966: Quasi-geostrophic motions in the equatorial area. *J. Meteor. Soc. Japan, Ser. II*, **44**, 25-43.
- Moskowitz, B. M.**, and C. S. Bretherton, 2000: An analysis of frictional feedback on a moist equatorial Kelvin mode. *J. Atmos. Sci.*, **57**, 2188-2206.
- Neelin, J. D.**, I. M. Held, and K. H. Cook, 1987: Evaporation-wind feedback and low-frequency variability in the tropical atmosphere. *J. Atmos. Sci.*, **44**, 2341-2348.
- Neelin, J. D.** and J.-Y. Yu, 1994: Modes of tropical variability under convective adjustment and the Madden-Julian oscillation. Part I: Analytical theory. *J. Atmos. Sci.*, **51**, 1876-1894.
- Raymond, D. J.**, 2000a: The Hadley circulation as a radiative-convective instability. *J. Atmos. Sci.*, **57**, 1286-1297.

- Raymond, D. J.**, 2000b: Thermodynamic control of tropical rainfall. *Quart. J. Roy. Meteor. Soc.*, **126**, 889-898.
- Raymond, D. J.**, 2001: A new model of the Madden-Julian oscillation. *J. Atmos. Sci.*, **58**, 2807-2819.
- Raymond, D. J.**, and M. Wilkening, 1985: Characteristics of mountain-induced thunderstorms and cumulus congestus clouds from budget measurements. *J. Atmos. Sci.*, **42**, 773-783.
- Raymond, D. J.**, and X. Zeng, 2005: Modeling tropical atmospheric convection in the context of the weak temperature gradient approximation. *Quart. J. Roy. Meteor. Soc.*, in press.
- Salby, M. L.**, R. R. Garcia, and H. H. Hendon, 1994: Planetary-scale circulations in the presence of climatological and wave-induced heating. *J. Atmos. Sci.*, **51**, 2344-2367.
- Sobel, A. H.**, and T. Horinouchi, 2000: On the dynamics of easterly waves, monsoon depressions, and tropical depression type disturbances. *J. Meteor. Soc. Japan*, **78**, 167-173.
- Sobel, A. H.**, J. Nilsson, and L. M. Polvani, 2001: The weak temperature gradient approximation and balanced tropical moisture waves. *J. Atmos. Sci.*, **58**, 3650-3665.
- Sobel, A. H.**, and C. S. Bretherton, 2003: Large-scale waves interacting with deep convection. *Tellus*, **55A**, 45-60.
- Straub, K. H.**, and G. N. Kiladis, 2002: Observations of a convectively coupled Kelvin wave in the Eastern Pacific ITCZ. *J. Atmos. Sci.*, **59**, 30-53.

- Tompkins**, A. M., and G. C. Craig, 1998: Radiative-convective equilibrium in a three-dimensional cloud-ensemble model. *Quart. J. Roy. Meteor. Soc.*, **124**, 2073-2097.
- Wang**, B., 1988: Dynamics of tropical low-frequency waves: An analysis of the moist Kelvin wave. *J. Atmos. Sci.*, **45**, 2051-2065.
- Wang**, B., and H. Rui, 1990: Dynamics of the coupled moist Kelvin-Rossby wave on an equatorial beta plane. *J. Atmos. Sci.*, **47**, 397-413.
- Wheeler**, M., and G. N. Kiladis, 1999: Convectively coupled equatorial waves: Analysis of clouds and temperature in the wavenumber-frequency domain. *J. Atmos. Sci.*, **56**, 374-399.
- Wheeler**, M., G. N. Kiladis, and P. J. Webster, 2000: Large-scale dynamical fields associated with convectively coupled equatorial waves. *J. Atmos. Sci.*, **57**, 613-639.
- Yano**, J., and K. A. Emanuel, 1991: An improved model of the equatorial troposphere and its coupling with the stratosphere. *J. Atmos. Sci.*, **48**, 377-389.

Table 1: Numerical values of parameters

Dimensional parameter	Symbol	Value
depth of the troposphere	h	15 km
free Kelvin wave speed	c	48 m/s
moisture relaxation rate	α	$1.2 \times 10^{-5} \text{s}^{-1}$
square of the Brunt Vaisala frequency	Γ_B	10^{-4}s^{-2}
moist static stability	Γ_E	10^{-5}s^{-2}
Dimensionless parameter	Symbol	Value
static stability	Γ	-0.1
scaled df/dy	β	10
buoyancy relaxation rate	μ	0
moisture and buoyancy relaxation	σ	1
cloud-radiative feedback parameter	ε	0.2
wind induced variations in surface fluxes	Λ	-0.4

Table 2: Nondimensionalization relationships, the first row represents the expression that becomes nondimensionalized parameter in the second row

αt	$\alpha x/c$	$\alpha y/c$	u/c	v/c	p/c^2	$\beta c/\alpha^2$	mz	b/mc^2	mw/α	q/mc^2	e/mc^2
t	x	y	u	v	p	β	z	b	w	q	e

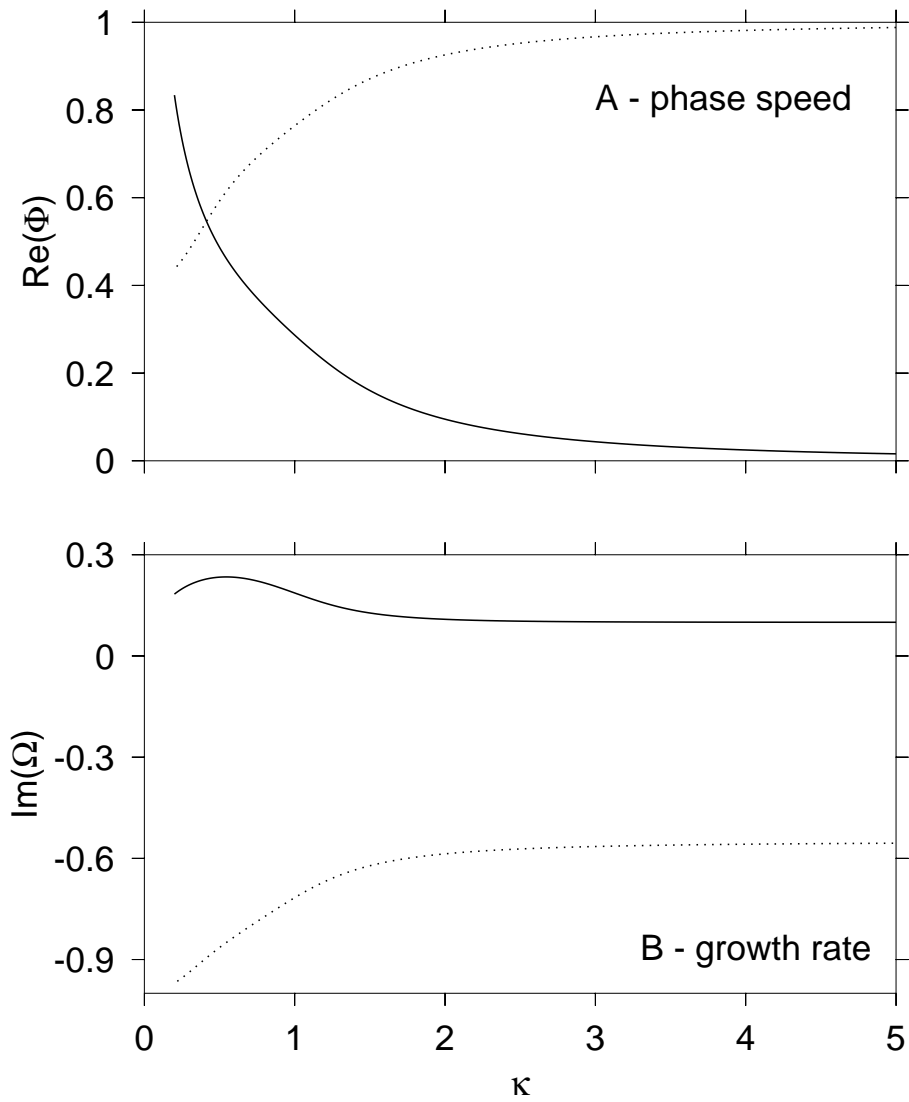


Figure 1: Combined CRI-WISHE case in rotating atmosphere for modes with $v(x, y) = 0$: dotted line is a Kelvin wave like mode and the solid line is an unstable slow moisture mode.

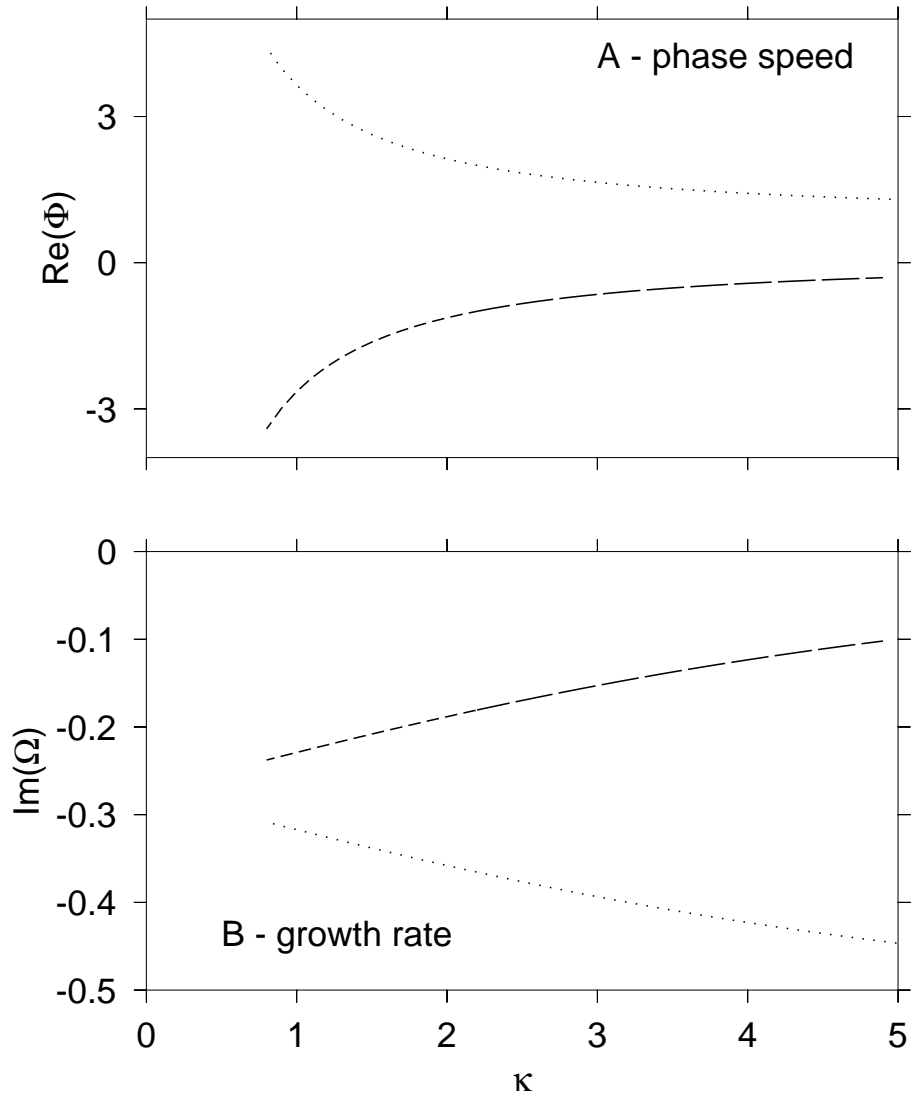


Figure 2: Combined CRI-WISHE case in rotating atmosphere for $n = 0$: dotted line represents the eastward propagating mixed Rossby-gravity wave, dashed line, westward propagating mixed Rossby-gravity wave.

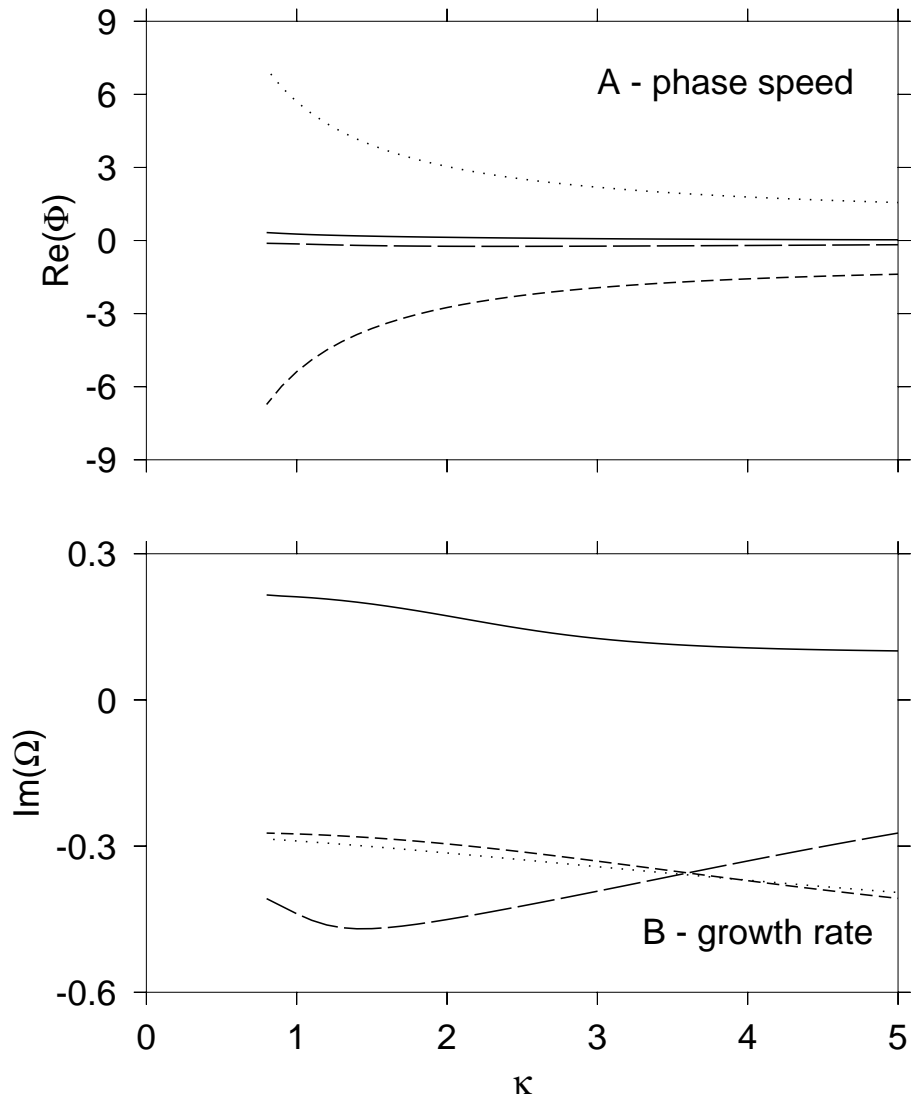


Figure 3: Combined CRI-WISHE case in rotating atmosphere for $n = 1$: dotted line represents the eastward propagating inertio-gravity wave. Short dashed line is westward propagating inertio-gravity wave while long dashed line is Rossby wave. The solid line is an unstable slow moisture mode.

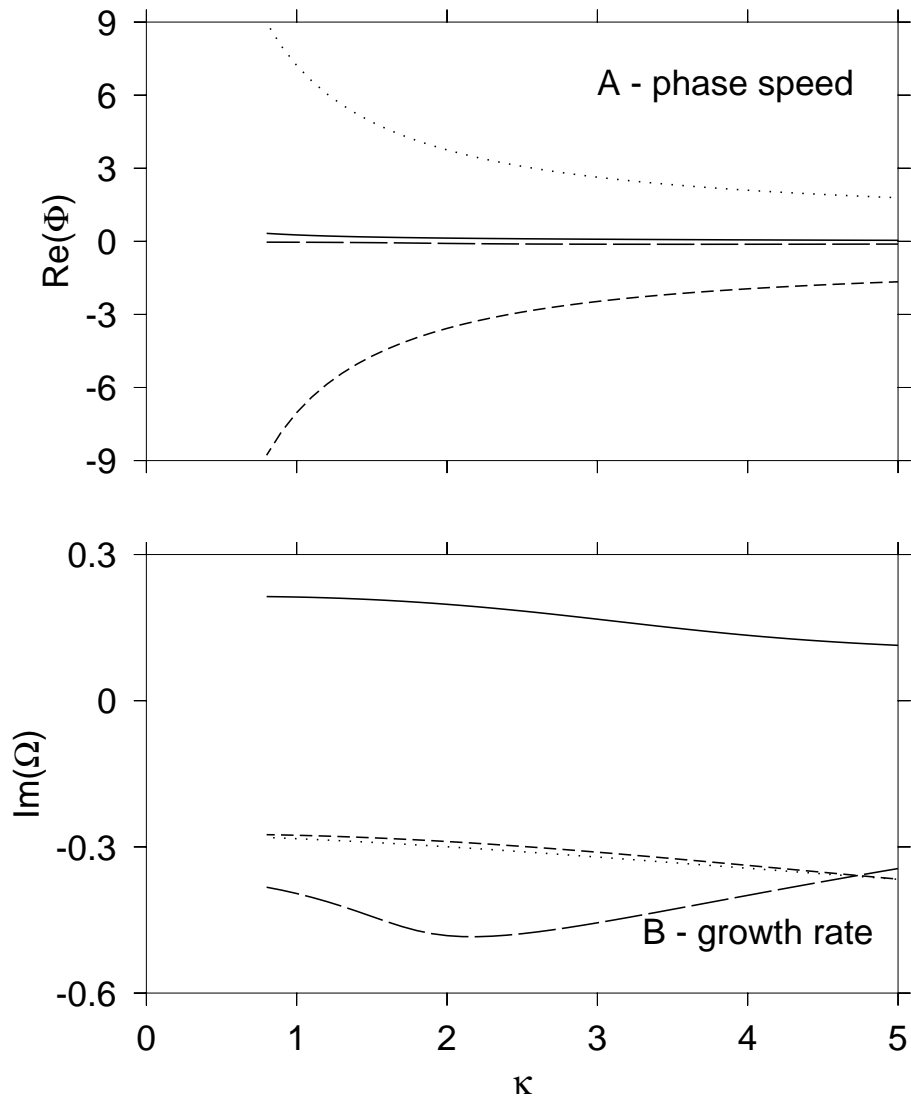


Figure 4: Same as Figure 3 only for $n = 2$.

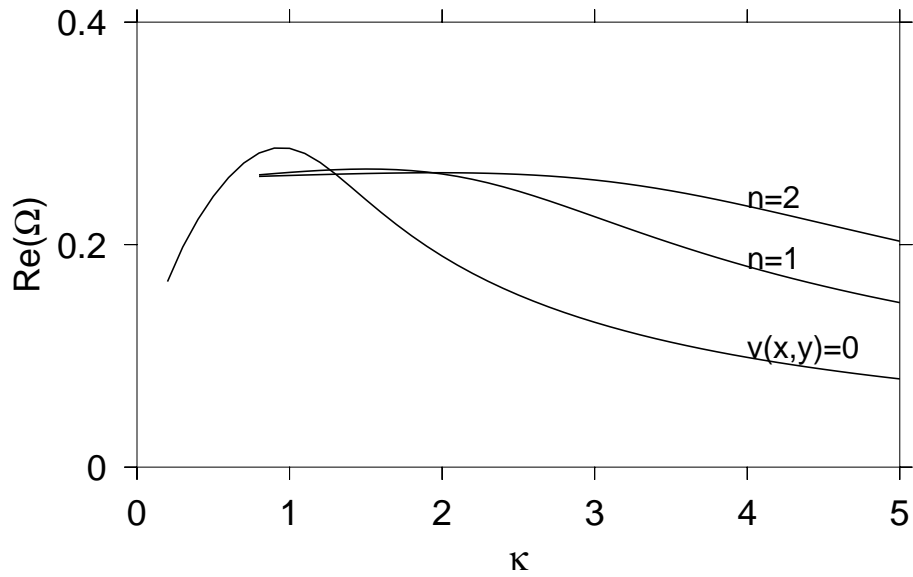


Figure 5: Real part of frequency for slow moisture mode versus wavenumber for combined CRI-WISHE case.

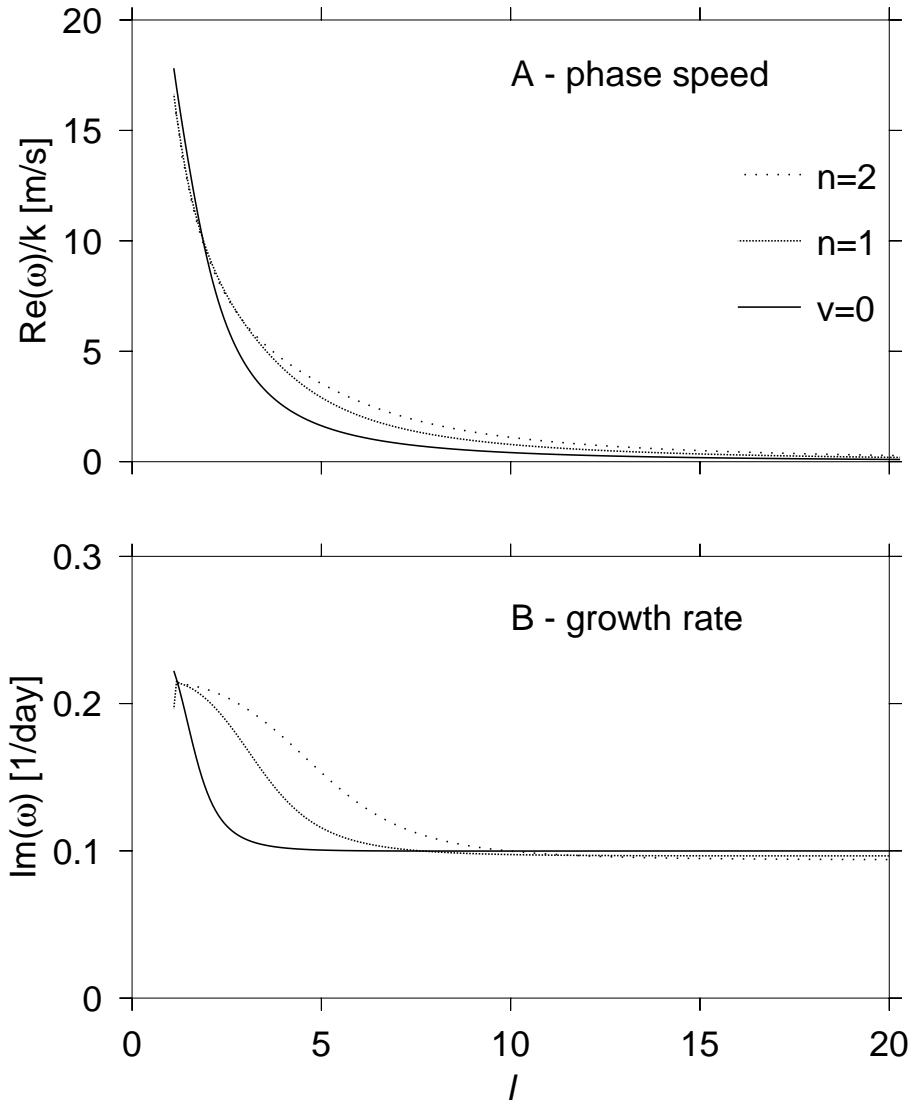


Figure 6: Dimensional dispersion curves of the slow moisture modes for combined CRI-WISHE case as a function of the planetary wavenumber l .

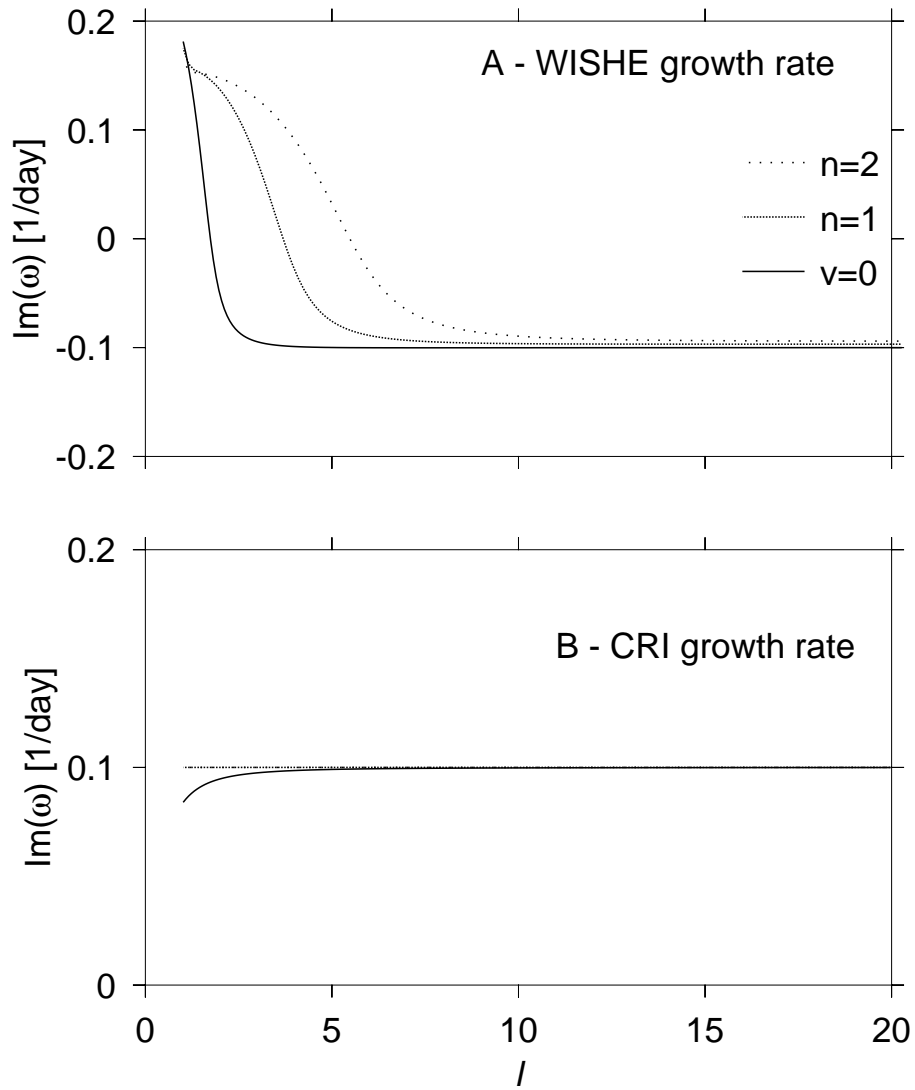


Figure 7: Dimensional growth rate of the slow moisture modes as a function of the planetary wavenumber l , plot A with WISHE only, plot B with CRI only.

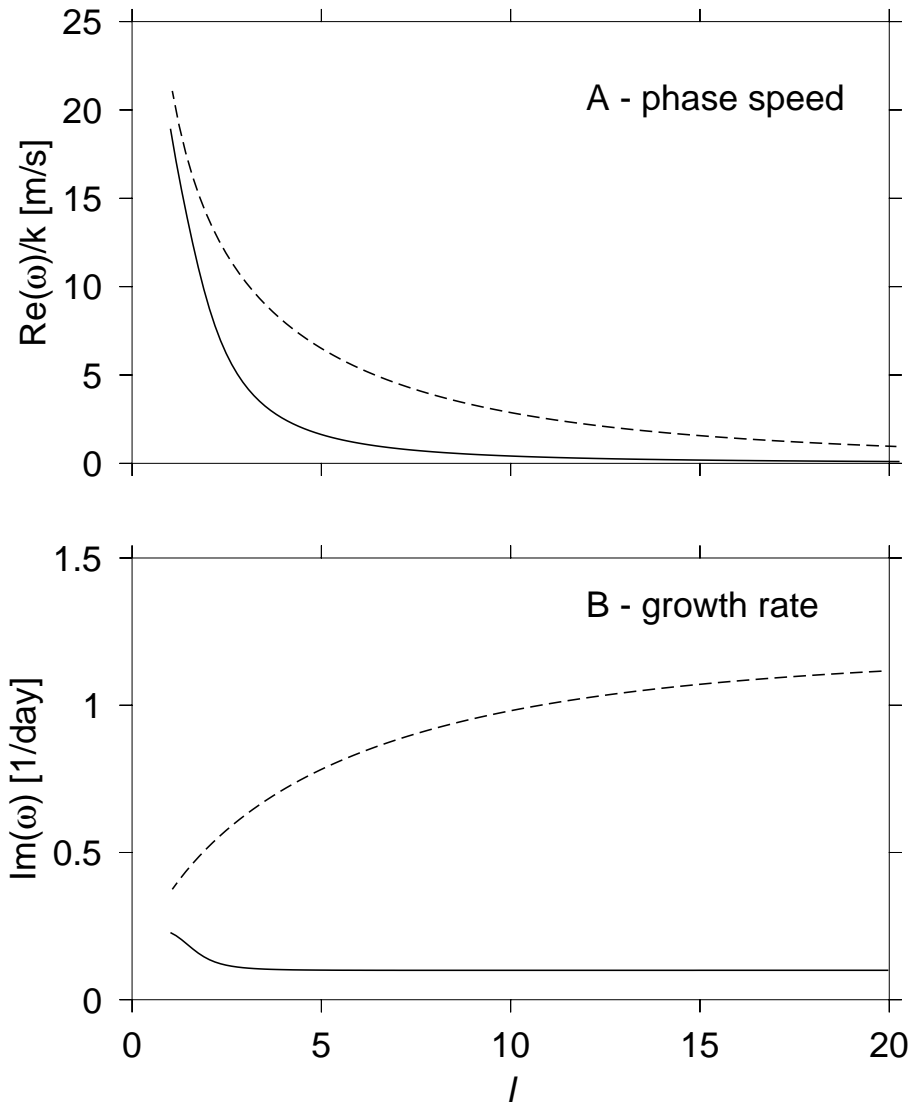


Figure 8: Dimensional dispersion curves of the slow moisture mode as a function of the planetary wavenumber l , for combined CRI-WISHE case when $v = 0$ for two time-scales: solid line corresponds to $\alpha^{-1} = 1$ day and the dashed line has $\alpha^{-1} = 2$ h.

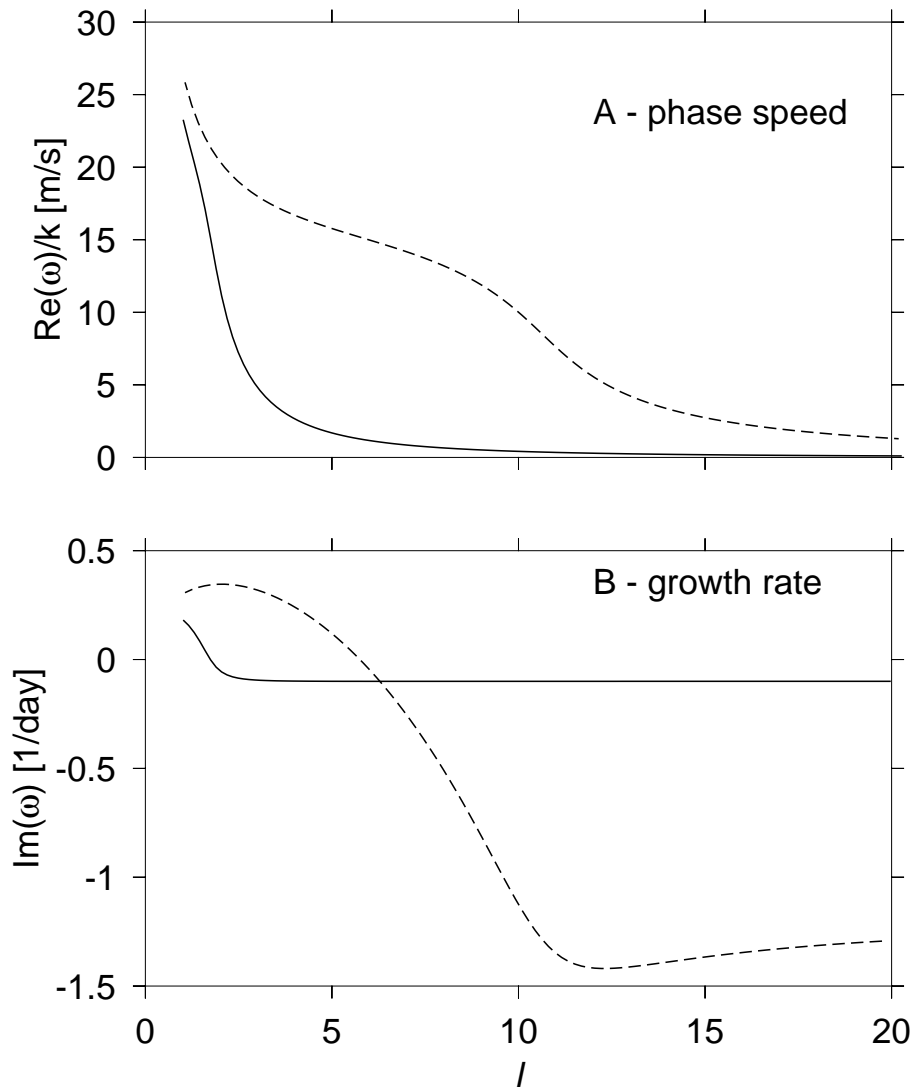


Figure 9: Same as Figure 8, only for WISHE without CRI.

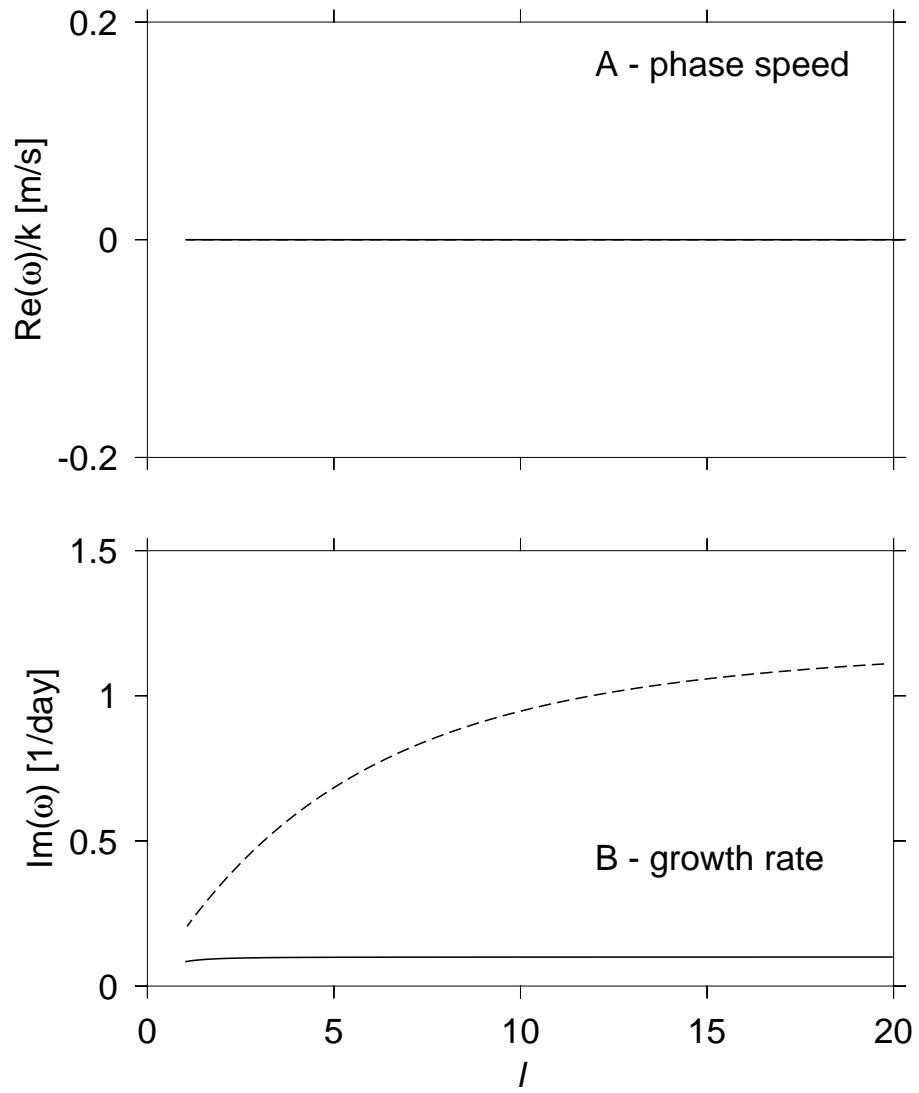


Figure 10: Same as Figure 8, for CRI without WISHE.

Table Captions

1. Numerical values of parameters.
2. Nondimensionalization relationships, the first row represents the expression that becomes nondimensionalized parameter in the second row.

Figure Captions

1. Combined CRI-WISHE case in rotating atmosphere for modes with $v(x, y) = 0$: dotted line is a Kelvin wave like mode and the solid line is an unstable slow moisture mode.
2. Combined CRI-WISHE case in rotating atmosphere for $n = 0$: dotted line represents the eastward propagating mixed Rossby-gravity wave, dashed line, westward propagating mixed Rossby-gravity wave.
3. Combined CRI-WISHE case in rotating atmosphere for $n = 1$: dotted line represents the eastward propagating inertio-gravity wave. Short dashed line is westward propagating inertio-gravity wave while long dashed line is Rossby wave. The solid line is an unstable slow moisture mode.
4. Same as Figure 3 only for $n = 2$.
5. Real part of frequency for slow moisture mode versus wavenumber for combined CRI-WISHE case.
6. Dimensional dispersion curves of the slow moisture modes for combined CRI-WISHE case as a function of the planetary wavenumber l .
7. Dimensional growth rate of the slow moisture modes as a function of the planetary wavenumber l , plot A with WISHE only, plot B with CRI only.
8. Dimensional dispersion curves of the slow moisture mode as a function of the planetary wavenumber l , for combined CRI-WISHE case when $v = 0$ for two time-scales: solid line corresponds to $\alpha^{-1} = 1$ day and the dashed line has $\alpha^{-1} = 2$ h.
9. Same as Figure 8, only for WISHE without CRI.

10. Same as Figure 8, for CRI without WISHE.